Publication V

Charles L. Dezelah IV, Pia Myllymäki, Jani Päiväsaari, Kai Arstila, Lauri Niinistö, and Charles H. Winter. 2007. The growth of $Er_xGa_{2-x}O_3$ films by atomic layer deposition from two different precursor systems. Journal of Materials Chemistry, volume 17, number 13, pages 1308-1315.

The growth of $Er_xGa_{2-x}O_3$ films by atomic layer deposition from two different precursor systems

Charles L. Dezelah IV,[a] Pia Myllymäki,[a] Jani Päiväsaari,[a] Kai Arstila,[b] Lauri Niinistö[a] and Charles H. Winter*[c]

Received 10th November 2006, Accepted 12th December 2006
First published as an Advance Article on the web 12th January 2007
DOI: 10.1039/b616443a

The atomic layer deposition (ALD) growth of $Er_xGa_{2-x}O_3$ ($0 \leqslant x \leqslant 2$) thin films was demonstrated using two precursor systems: $Er(thd)_3$, $Ga(acac)_3$, and ozone and $Er(C_5H_4Me)_3$, $Ga_2(NMe_2)_6$, and water at substrate temperatures of 350 and 250 °C, respectively. Both processes provided uniform films and exhibited surface-limited ALD growth. The value of x in $Er_xGa_{2-x}O_3$ was easily varied by selecting a pulse sequence with an appropriate erbium to gallium precursor ratio. The $Er(thd)_3$, $Ga(acac)_3$, and ozone precursor system provided stoichiometric $Er_xGa_{2-x}O_3$ films with carbon, hydrogen, nitrogen, and fluorine levels of <0.2, <0.2, <0.3, and 0.6–2.2 atomic percent, respectively, as determined by Rutherford backscattering spectrometry (RBS) and time of flight-elastic recoil detection analysis (TOF-ERDA). The film growth rate was between 0.25 and 0.28 Å cycle^{-1}. The effective permittivity of representative samples was between 10.8 and 11.3. The $Er(C_5H_4Me)_3$, $Ga_2(NMe_2)_6$, and water precursor system provided stoichiometric $Er_xGa_{2-x}O_3$ films with carbon, hydrogen, nitrogen, and fluorine levels of 2.0–6.1, 5.0–10.3, <0.3–0.7, and $\leqslant 0.1$ atom percent, respectively, as determined by RBS and TOF-ERDA. The film growth rate was between 1.0 and 1.5 Å cycle^{-1} and varied as a function of the $Er(C_5H_4Me)_3$ to $Ga_2(NMe_2)_6$ pulse ratio. The effective permittivity of representative samples was between 9.2 and 10.4. The as-deposited films of both precursor systems were amorphous, but crystallized either to $Er_3Ga_5O_{12}$ or to a mixture of β-Ga_2O_3 and $Er_3Ga_5O_{12}$ upon annealing between 900 and 1000 °C under a nitrogen atmosphere. Atomic force microscopy showed root mean square surface roughnesses of <1.0 nm for typical films regardless of precursor system or film composition.

Introduction

Lanthanide gallium oxides of the formula $Ln_xGa_{2-x}O_3$ have received considerable attention in recent years due to many potential applications, which include thin film wave guides,[1] substrate materials for epitaxial high T_c superconductor thin film growth,[2] as well as components in solid oxide fuel cells.[3] Perhaps the most prominent applications proposed for $Ln_xGa_{2-x}O_3$, however, are as passivating layers and dielectric materials for group 13–15 semiconductor devices,[4] especially those based on gallium arsenide (GaAs).[5] GaAs has been the subject of intense interest for use in metal-oxide-semiconductor field-effect transistors (MOSFETs) due to its significant advantages over silicon,[6] including higher saturated electron velocity, electron mobility, and breakdown voltages. These features allow operation at higher frequency and power than traditional silicon/SiO_2-based microelectronics. A major obstacle to the wider use of GaAs is the difficulty of finding a suitable passivating dielectric material.[7] Gadolinium gallium oxide ($Gd_xGa_{2-x}O_3$) has emerged recently as an important candidate material to serve in this capacity, since it possesses good stability, a low interfacial density of states, and a suitable dielectric constant.[5]

A limiting factor in the implementation of $Ln_xGa_{2-x}O_3$ is the development of practical and functional routes to thin film growth, and only a few examples of routes to these materials have been reported. $Gd_xGa_{2-x}O_3$ has been previously deposited using molecular beam epitaxy.[5] The growth of $LaGaO_3$ thin films has been described using a sol–gel method,[8] and both $LaGaO_3$ and $NdGaO_3$ films have been grown by RF magnetron sputtering.[9] $NdGaO_3$[10] and $PrGaO_3$[11] film growth has been reported using metalorganic chemical vapor deposition. The atomic layer deposition (ALD) growth of $La_xGa_{2-x}O_3$ has also been described employing tris(2,2,4,4-tetramethyl-3,5-heptanedionato)lanthanum ($La(thd)_3$) and tris(acetylacetonato)gallium ($Ga(acac)_3$) as metalorganic precursors and ozone as the oxidant.[12] Of the many possible thin film growth methods, ALD has been identified as one of the most promising manufacturing techniques for future microelectronics devices, since it can provide thin films with controlled thickness as well as perfect conformal coverage.[13] ALD film growth entails exposure of the substrate surface to sequential pulses of two or more precursors, which are separated by inert gas purges to remove excess precursor and also to remove the reaction byproducts. To have maximum utility in ALD growth, a metal-containing precursor must be thermally stable on the surface of the substrate at the film growth temperature, but also must react rapidly and efficiently

[a]*Laboratory of Inorganic and Analytical Chemistry, Helsinki University of Technology, P.O. Box 6100, FI-02015, Espoo, Finland*
[b]*IMEC, Kapeldreef 75, B-3001, Leuven, Belgium*
[c]*Department of Chemistry, Wayne State University, 5101 Cass Avenue, Detroit, Michigan, 48202, USA. E-mail: chw@chem.wayne.edu*

with a second reagent to provide the desired material. To date, the ALD growth of $Gd_xGa_{2-x}O_3$ films has remained elusive due to the lack of suitable Gd_2O_3 and Ga_2O_3 ALD precursors with compatible processing windows. Given the excellent potential of the other Ln_2O_3 phases to serve as effective high-κ dielectrics,[14] the development of new ALD processes for other $Ln_xGa_{2-x}O_3$ could offer alternative passivating dielectric materials for gallium arsenide.

Herein, we describe the ALD growth of $Er_xGa_{2-x}O_3$ films from two different precursor systems: tris(2,2,4,4-tetramethyl-3,5-heptanedionato)erbium ($Er(thd)_3$), $Ga(acac)_3$, and ozone, and tris(methylcyclopentadienyl)erbium ($Er(C_5H_4Me)_3$), hexakis(dimethylamido)digallium ($Ga_2(NMe_2)_6$), and water. $Er(thd)_3$[15] and $Ga(acac)_3$[16] have been reported to afford surface-limited ALD growth of Er_2O_3 and Ga_2O_3 films, respectively, when operating at a deposition temperature of 350 °C and using ozone as the oxygen source. In addition, $Er(C_5H_4Me)_3$[17] and $Ga_2(NMe_2)_6$[18] afford ALD growth of Er_2O_3 and Ga_2O_3 films, respectively, at 250 °C with water as the oxygen source. ALD growth of ternary materials requires overlap of the temperature windows at which surface-limited growth is obtained for the two binary deposition processes.[13] Thus, we have combined these aforementioned Er_2O_3 and Ga_2O_3 ALD processes to afford efficient surface-limited ALD growth of $Er_xGa_{2-x}O_3$ films.

Results

$Er_xGa_{2-x}O_3$ film growth studies

The deposition of $Er_xGa_{2-x}O_3$ thin films by ALD was studied using the precursors $Er(thd)_3$, $Ga(acac)_3$, and ozone and $Er(C_5H_4Me)_3$, $Ga_2(NMe_2)_6$, and water. The relative amounts of erbium and gallium were adjusted by varying the pulse ratios of the individual binary processes. Deposition experiments using $Er(thd)_3$, $Ga(acac)_3$, and ozone were performed at 350 °C and those employing $Er(C_5H_4Me)_3$, $Ga_2(NMe_2)_6$, and water were performed at 250 °C. These temperatures reflect those at which the parent processes have overlapping ALD windows and exhibit surface-controlled growth behavior.[15,16] The pulse lengths for each precursor and the purge lengths separating the pulses were established by first selecting the ones that were used for the binary Er_2O_3 and Ga_2O_3 processes, and then testing whether an increase in the pulse lengths of the erbium or gallium precursors resulted in an increase in the growth rate of the film. A central feature of ALD growth is the saturation of the substrate surface with each precursor pulse.[13] When this condition is satisfied, growth is surface-limited and doses beyond the minimal amount necessary for surface saturation do not result in an increase in growth rate. Pulse lengths of $\geqslant$1.0 s for both $Er(thd)_3$ and $Ga(acac)_3$ and $\geqslant$1.5 s for ozone afforded surface-limited growth for the process using these precursors. Pulse lengths of $\geqslant$1.0 s, $\geqslant$1.5 s, and $\geqslant$1.5 s for $Er(C_5H_4Me)_3$, $Ga_2(NMe_2)_6$, and water, respectively, resulted in surface-limited growth for the process employing these precursors. Because $Er_xGa_{2-x}O_3$ can possess a range of possible compositions, experiments were carried out where the ratios of erbium : gallium precursor pulses were varied. Fig. 1 depicts the relationship between the erbium pulse percentage and both the erbium content (as determined by X-ray fluorescence spectroscopy, XRF) and growth rate of films deposited using $Er(thd)_3$, $Ga(acac)_3$, and ozone. The erbium : gallium ratio in the films increased with increasing erbium pulse percentages. The increase was nearly linear when using erbium pulse percentages in the range of 0–50%, but the slope increased for more erbium-rich films. The growth rate of $Er_xGa_{2-x}O_3$ (0.25–0.28 Å cycle^{-1}) did not vary with the percentage of erbium pulses and was identical to the parent binary processes within experimental error. Fig. 2 depicts the relationship between the erbium pulse percentage and both composition and film growth rate using $Er(C_5H_4Me)_3$, $Ga_2(NMe_2)_6$, and water. Again, the erbium content increased with increasing erbium pulse percentage. The increase was nearly linear over much of the range, but a higher slope was observed as the erbium percentage exceeded 75%. The growth rate of films (0.95–1.00 Å cycle^{-1}) closely resembled the growth rate of the parent Ga_2O_3 process for erbium pulse percentages of up to about 70%.[18] As the amount of erbium present in the films exceeded 75%, the growth rate increased from about 1 Å cycle^{-1} to about 1.5 Å cycle^{-1}. The latter growth rate equals that of the binary Er_2O_3 process.[17]

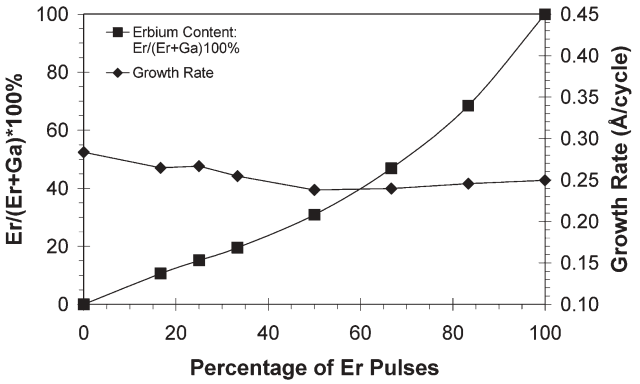

Fig. 1 Film composition (as determined by XRF) and growth rate plotted as a function of the precursor pulse ratio (expressed as the percentage of the total number of metal precursor pulses that were erbium precursor pulses) for the $Er(thd)_3$, $Ga(acac)_3$, and ozone process.

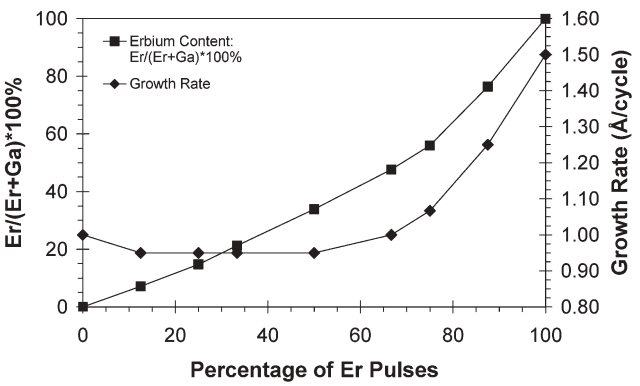

Fig. 2 Film composition and growth rate plotted as a function of the precursor pulse ratio (expressed as the percentage of the total number of metal precursor pulses that were erbium precursor pulses) for the $Er(C_5H_4Me)_3$, $Ga_2(NMe_2)_6$, and water process.

Table 1 Elemental composition of $Er_xGa_{2-x}O_3$ thin films in atomic percentages as determined by RBS and TOF-ERDA

Precursor system	Pulse ratio (Er : Ga)	%Er	%Ga	%O	%C	%H	%N	%F
$Er(C_5H_4Me)_3$, $Ga_2(NMe_2)_6$, water	1 : 3	6.1 ± 1.0	28.9 ± 3.0	48.2 ± 5.0	6.1 ± 2.0	9.9 ± 2.0	0.7 ± 0.3	0.1 ± 0.1
	1 : 1	13.3 ± 2.0	21.7 ± 3.0	49.1 ± 5.0	5.6 ± 2.0	10.3 ± 2.0	<0.3	<0.1
	3 : 1	23.5 ± 3.0	15.3 ± 2.0	54.3 ± 5.0	2.0 ± 2.0	5.0 ± 2.0	<0.3	<0.1
$Er(thd)_3$, $Ga(acac)_3$, ozone	1 : 3	7.3 ± 1.0	33.2 ± 3.0	58.8 ± 5.0	<0.2	<0.2	<0.3	0.6 ± 0.2
	1 : 1	14.5 ± 2.0	26.3 ± 3.0	58.0 ± 5.0	<0.2	<0.2	<0.3	1.2 ± 0.2
	11 : 5	22.0 ± 3.0	17.4 ± 2.0	58.4 ± 5.0	<0.2	<0.2	<0.3	2.2 ± 0.4

Table 2 Overview of data calculated from the RBS and TOF-ERDA compositional analyses

Precursor system	Pulse ratio (Er : Ga)	M : O ratio	Er : Ga ratio	x ($Er_xGa_{2-x}O_3$, $0 \leqslant x \leqslant 2$)	[Er/(Er + Ga)] × 100%
$Er(C_5H_4Me)_3$, $Ga_2(NMe_2)_6$, water	1 : 3	0.73 ± 0.10	0.21 ± 0.04	0.35 ± 0.07	17.4 ± 3.3
	1 : 1	0.71 ± 0.10	0.61 ± 0.13	0.76 ± 0.14	38.0 ± 6.9
	3 : 1	0.71 ± 0.09	1.53 ± 0.28	1.21 ± 0.19	60.6 ± 9.6
$Er(thd)_3$, $Ga(acac)_3$, ozone	1 : 3	0.69 ± 0.08	0.22 ± 0.04	0.36 ± 0.06	18.0 ± 2.8
	1 : 1	0.70 ± 0.09	0.55 ± 0.10	0.71 ± 0.12	35.5 ± 5.8
	11 : 5	0.67 ± 0.08	1.26 ± 0.23	1.12 ± 0.18	55.8 ± 9.2

Characterization of $Er_xGa_{2-x}O_3$ films

A combination of Rutherford backscattering spectroscopy (RBS) and time-of-flight elastic recoil detection analysis (TOF-ERDA) was performed on representative $Er_xGa_{2-x}O_3$ films to determine the elemental compositions (Table 1). The films consisted of stoichiometric $Er_xGa_{2-x}O_3$ within experimental error. The value of x was adjusted by varying the erbium : gallium precursor pulse ratio. The ratio of metal to oxygen was 0.69, 0.70, and 0.67 for films deposited using $Er(thd)_3$: $Ga(acac)_3$ pulse ratios of 1 : 3, 1 : 1, and 11 : 5, respectively (Table 2). The ratio of metal to oxygen was 0.73, 0.71, and 0.71 for films deposited with $Er(C_5H_4Me)_3$: $Ga_2(NMe_2)_6$ pulse ratios of 1 : 3, 1 : 1, and 3 : 1, respectively. The amount of erbium present in samples made from either precursor set increased with increasing erbium : gallium pulse ratios (Table 2), with a trend that is consistent with that observed in the XRF compositional studies depicted in Fig. 1 and 2. The concentration of impurity elements was determined by TOF-ERDA (Table 1). Representative film samples from $Er(thd)_3$, $Ga(acac)_3$, and ozone had carbon, hydrogen, and nitrogen concentrations that were below detection limits (<0.2, <0.2, and <0.3 atomic percent, respectively). Fluorine concentrations for these samples were between 0.6 and 2.2 atomic percent, and increased with higher erbium : gallium pulsing ratios. Impurity levels were higher in films grown using $Er(C_5H_4Me)_3$, $Ga_2(NMe_2)_6$, and water. The carbon concentration of representative samples was in the range of 2.0–6.1 atomic percent and decreased with an increase in the $Er(C_5H_4Me)_3$: $Ga_2(NMe_2)_6$ pulse ratio. Hydrogen levels followed a similar trend, and afforded concentrations of 5.0–10.3 atomic percent. A film deposited using the highest $Er(C_5H_4Me)_3$: $Ga_2(NMe_2)_6$ pulse ratio (3 : 1) produced the lowest carbon and hydrogen levels. Nitrogen concentrations were below detection limits (0.3 atomic percent) for all samples except for the one deposited using a 1 : 3 $Er(C_5H_4Me)_3$: $Ga_2(NMe_2)_6$ pulse ratio, for which the nitrogen concentration was 0.7 atomic percent. The RBS/TOF-ERDA analyses did not reveal significant compositional variations as a function of depth for the samples examined.

X-Ray diffraction (XRD) was performed on films deposited from $Er(thd)_3$, $Ga(acac)_3$, and ozone using a range of erbium : gallium precursor pulse ratios to determine the presence of any crystalline phases. XRD measurements showed no clear diffraction peaks for any of the as-deposited film samples, which indicated amorphous structures. However, crystallization occurred upon annealing to 900–1000 °C under nitrogen (Fig. 3). After heating an amorphous $Er_xGa_{2-x}O_3$ film to 1000 °C that was deposited using an 11 : 5 $Er(thd)_3$: $Ga(acac)_3$ pulse ratio, reflections were observed in the XRD pattern at 2θ = 17.5, 26.9, 28.7, 32.2, 35.4, 36.9, 39.7, 44.9, 50.9, 53.1, 54.2, 55.3, and 59.4°. These values correspond respectively to reflections from the following planes of the known phase $Er_3Ga_5O_{12}$: (211), (321), (400), (420), (422), (431), (521), (661),

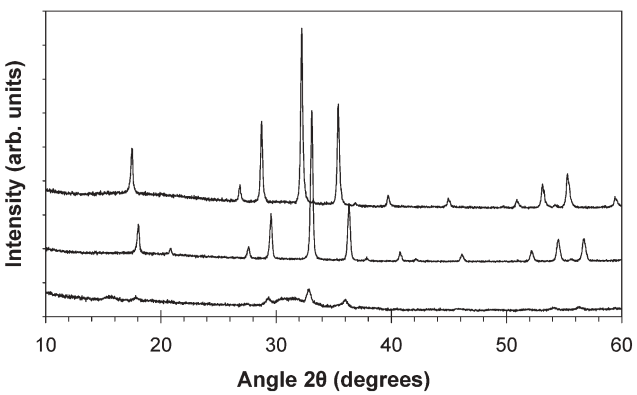

Fig. 3 X-Ray diffraction patterns collected for representative annealed $Er_xGa_{2-x}O_3$ films deposited with erbium : gallium pulse ratios of 11 : 5 (top), 1 : 1 (middle), and 3 : 10 (bottom) using $Er(thd)_3$, $Ga(acac)_3$, and ozone as precursors. The temperatures used for annealing were 1000, 900, and 900 °C, respectively, and represent the temperatures at which crystallization was first observed. All films were amorphous as deposited.

(444), (640), (721), (642), and (800).[19] Annealing of the film at lower temperatures did not result in crystallization. Annealing of an $Er_xGa_{2-x}O_3$ film to 900 °C that was deposited using a 1 : 1 $Er(thd)_3$: $Ga(acac)_3$ pulse ratio resulted in a diffraction pattern that was very similar to the one described above, but with the following differences: (1) two additional reflections were observed at 2θ = 20.9 and 42.1°, which correspond to the (220) and (440) reflections of $Er_3Ga_5O_{12}$, respectively, and (2) each reflection exhibited a shift to a higher value of 2θ (or lower *d*-spacing) relative to the film deposited using an 11 : 5 $Er(thd)_3$: $Ga(acac)_3$ pulse ratio. Shifts in the 2θ values were in the range of 0.5–1.7° (approximately 0.04–0.15 Å *d*-spacing shifts), with greater 2θ shifts observed for reflections occurring at larger 2θ values. This behavior equates to smaller *d*-spacing shifts for reflections from sets of planes exhibiting smaller *d*-spacing values, where the shift corresponds to a 2.5 ± 0.3% reduction in *d*-spacing for each of the reflections observed, and may result from some replacement of erbium ion by the smaller gallium ion. Annealing to 900 °C of an $Er_xGa_{2-x}O_3$ film deposited using a 3 : 10 $Er(thd)_3$: $Ga(acac)_3$ pulse ratio resulted in a diffraction pattern containing only broad low-intensity reflections. The observed reflections are consistent with the presence of both $Er_3Ga_5O_{12}$ and β-Ga_2O_3. The reflections at 2θ = 15.7, 19.1, 30.4, 31.7, and 48.6° index as the (100), (−102), (−104), (−202), and (015) reflections of β-Ga_2O_3, respectively.[19] Reflections consistent with those expected for the (211), (321), (400), (420), (422), (521), (611), (444), (640), and (642) planes of $Er_3Ga_5O_{12}$ were also present.[19]

A similar XRD annealing study was performed on films grown using $Er(C_5H_4Me)_3$, $Ga_2(NMe_2)_6$, and water (Fig. 4). No clear diffraction peaks were observed for any of the as-deposited film samples, but crystallization did occur upon annealing. After heating an amorphous $Er_xGa_{2-x}O_3$ film to 900 °C that was deposited using a 1 : 1 $Er(C_5H_4Me)_3$: $Ga_2(NMe_2)_6$ pulse ratio, reflections were observed in the XRD spectrum at 2θ = 18.1, 27.5, 29.5, 33.1, 36.3, 40.8, 46.0, 52.1, 54.3, and 56.6°. These values correspond reflections arising from the (211), (321), (400), (420), (422), (521), (661), (444), (640), and (642) planes of $Er_3Ga_5O_{12}$.[19] Annealing of this film at lower temperatures did not result in crystallization. An $Er_xGa_{2-x}O_3$ film that was grown with a 3 : 1 $Er(C_5H_4Me)_3$: $Ga_2(NMe_2)_6$ pulse ratio and then annealed at 1000 °C afforded a diffraction pattern containing reflections consistent with $Er_3Ga_5O_{12}$ and β-Ga_2O_3. Reflections due to $Er_3Ga_5O_{12}$ were observed at 2θ = 17.7, 20.4, 27.2, 29.1, 33.0, 35.8, 40.2, 53.7, and 55.9°, which are consistent with those expected for the (221), (220) (321), (400), (420), (422), (521), (640), and (642) planes, respectively.[19] Reflections consistent with β-Ga_2O_3 appeared at 2θ = 15.9, 19.3, 29.9, and 31.4°, which index as the (100), (−102), (−104), and (−202) planes, respectively. Reflections at 2θ = 42.5, 44.1, 46.9, and 49.3° were too broad and of too low intensity to be unambiguously identified, but probably originate from either $Er_3Ga_5O_{12}$ or β-Ga_2O_3 planes expected to appear in this region.[19] Annealing of an $Er_xGa_{2-x}O_3$ film at 1000 °C that was deposited using a 1 : 3 $Er(C_5H_4Me)_3$: $Ga_2(NMe_2)_6$ pulse ratio resulted in a diffraction pattern containing no discernable reflections, which indicates that the film remained amorphous despite annealing at a high temperature.

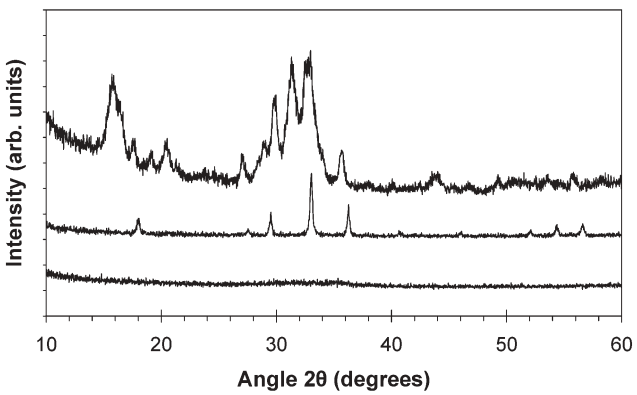

Fig. 4 X-Ray diffraction patterns collected for representative annealed $Er_xGa_{2-x}O_3$ films deposited erbium : gallium pulse ratios of 3 : 1 (top), 1 : 1 (middle), and 1 : 3 (bottom) using $Er(C_5H_4Me)_3$, $Ga_2(NMe_2)_6$, and water as precursors. The temperatures used for annealing were 1000, 900, and 1000 °C, respectively, and represent the temperatures at which crystallization was first observed. All films were amorphous as deposited.

The surface morphology of the as-deposited films was studied by atomic force microscopy (AFM). Micrographs of characteristic film surface features were collected for $Er_xGa_{2-x}O_3$ films deposited with both precursor sets and a variety of precursor pulse ratios. The as-deposited films were smooth and featureless with root mean square (rms) surface roughnesses of <1.0 nm for typical 2 μm × 2 μm areas. Fig. 5 depicts AFM images of two representative $Er_xGa_{2-x}O_3$ films, for which the measured rms surface roughness values were 0.4 and 0.6 nm.

Capacitance–voltage (*C–V*) curves were measured for Al/$Er_xGa_{2-x}O_3$/SiO_2/p-Si(100) capacitor structures containing 48.6 and 45.6 nm thick $Er_xGa_{2-x}O_3$ films grown using $Er(thd)_3$: $Ga(acac)_3$ pulse ratios of 1 : 3 and 11 : 5. These depositions afforded $Er_xGa_{2-x}O_3$ with x = 0.36 and 1.12, respectively (Fig. 6). For the film where x = 1.12, the flat band voltage shift (V_{fb}) was −1.3 V, which is close to the shift (−1.0 V) that is characteristic of Al/insulator/p-Si(100) structures.[20] A film having a smaller amount of erbium (x = 0.36) exhibited a V_{fb} of −0.3 V, which represents a shift toward positive bias relative to the expected position, suggesting the presence of negative fixed charge in the film. The hysteresis (ΔV_{fb}) was small for both *C–V* curves (~15 mV), which suggests that the number of charge traps in the film or at the film/SiO_2 interface is low. Permittivity values (κ) were 10.8 and 11.3, respectively, for films where x = 0.36 and 1.12. Both films displayed low leakage current density (16 nA cm^{-2} for each) at 1 V. *C–V* curves were also measured for capacitor structures with 41.4 and 42.6 nm thick $Er_xGa_{2-x}O_3$ films that were grown using 1 : 3 and 1 : 1 pulse ratios of $Er(C_5H_4Me)_3$: $Ga_2(NMe_2)_6$, to afford films where x = 0.35 and 0.76, respectively (Fig. 7). For the film where x = 0.76, the flat band voltage shift (V_{fb}) was −1.2 V, which is close to the shift (−1.0 V) that is characteristic of Al/insulator/p-Si(100) structures.[20] A film having a smaller amount of erbium (x = 0.35) exhibited a V_{fb} of −0.2 V, which represents a

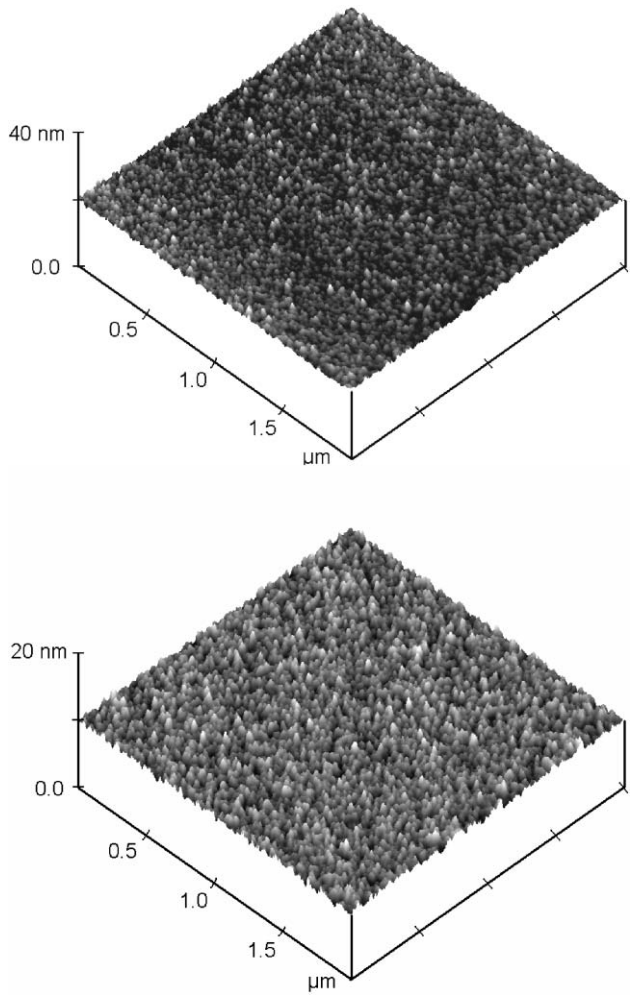

Fig. 5 Representative AFM images of $Er_xGa_{2-x}O_3$ thin films deposited by ALD using $Er(C_5H_4Me)_3$, $Ga_2(NMe_2)_6$, and water with an erbium : gallium pulse ratio of 1 : 1 (top; film thickness = 57 nm) and $Er(thd)_3$, $Ga(acac)_3$, and ozone with an erbium : gallium pulse ratio of 11 : 5 (bottom; film thickness = 46 nm). The measured rms values were 0.6 nm and 0.4 nm, respectively.

shift toward positive bias relative to the expected position, suggesting the presence of negative fixed charge in the film. The hysteresis (ΔV_{fb}) was significant for both *C–V* curves (>200 mV), which may be due to the presence of charge traps in the film or at the film/SiO_2 interface. Permittivity values (κ) were 9.2 and 10.4, respectively, for films where $x = 0.35$ and 0.76. The leakage current density was low for both film samples (26 and 17 nA cm^{-2} at 1 V for $x = 0.35$ and 0.76, respectively). The data collected from electrical characterization are summarized in Table 3.

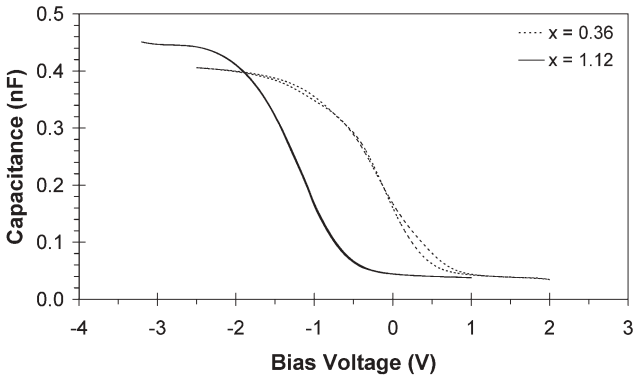

Fig. 6 Capacitance–voltage curves of Al/$Er_xGa_{2-x}O_3$/SiO_2/p-Si(100) capacitor structures with an $Er_xGa_{2-x}O_3$ film grown at 350 °C from $Er(thd)_3$, $Ga(acac)_3$, and ozone. For $x = 0.36$ and 1.12, the film thicknesses were 48.6 and 45.6 nm, respectively.

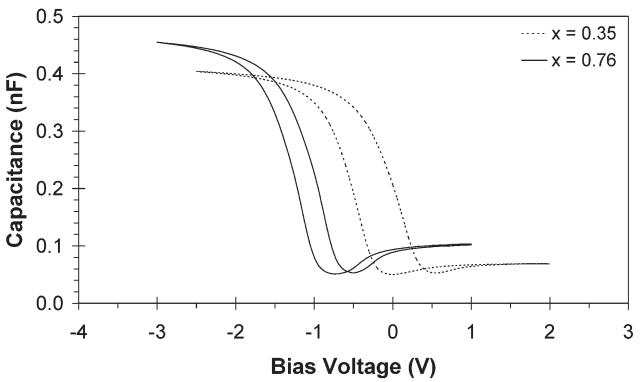

Fig. 7 Capacitance–voltage curves of Al/$Er_xGa_{2-x}O_3$/SiO_2/p-Si(100) capacitor structures with an $Er_xGa_{2-x}O_3$ film grown at 250 °C from $Er(C_5H_4Me)_3$, $Ga_2(NMe_2)_6$, and water. For $x = 0.35$ and 0.76, the film thicknesses were 41.4 and 42.6 nm, respectively.

Discussion

In this report, we describe the first examples of $Er_xGa_{2-x}O_3$ films to be grown by any method. In addition, only a few examples of other $Ln_xGa_{2-x}O_3$ films have been reported.[4,5,8–12] CVD approaches have been limited to the growth of $PrGaO_3$ and $NdGaO_3$, which were accessed using $Ln(thd)_3$, $Ga(thd)_3$, and N_2O as the metallic and oxidant source compounds, respectively.[10,11] The CVD-based processes required substrate temperatures of 750–800 °C, which far exceed the 500 °C upper limit proscribed for high-κ dielectric layers.[21] In addition, CVD-based processes cannot provide the same degree of thickness control and conformal coverage of patterned substrates as ALD. To date, the only

Table 3 Summary of electrical characterization

Precursor system	Pulse ratio (Er : Ga)	x ($Er_xGa_{2-x}O_3$, $0 \leqslant x \leqslant 2$)	κ	V_{fb}/V	ΔV_{fb}/mV	Leakage current density at 1 V/nA cm^{-2}
$Er(C_5H_4Me)_3$, $Ga_2(NMe_2)_6$, water	1 : 3	0.35 ± 0.07	9.2	−0.2	680	26
	1 : 1	0.76 ± 0.14	10.4	−1.2	250	17
$Er(thd)_3$, $Ga(acac)_3$, ozone	1 : 3	0.36 ± 0.06	10.8	−0.3	~15	16
	11 : 5	1.12 ± 0.18	11.3	−1.3	~15	16

previous example of an ALD-grown $Ln_xGa_{2-x}O_3$ film is $LaGaO_3$, which was reported by Nieminen *et al.*[12] This ALD process, like the CVD processes discussed above, employed β-diketonate precursors as the lanthanide and gallium sources. While the ozone-based process demonstrated herein afforded high purity $Er_xGa_{2-x}O_3$ films, use of ozone could lead to extensive formation of arsenic oxides at the GaAs/$Er_xGa_{2-x}O_3$ interface. Such oxides lead to high leakage currents,[5] so ozone-based ALD processes may be less useful for $Ln_xGa_{2-x}O_3$ film growth in GaAs-based devices. In envisioning water-based ALD approaches to $Ln_xGa_{2-x}O_3$ films, we considered the growth of $Gd_xGa_{2-x}O_3$ from a process involving $Gd(C_5H_4Me)_3$, $Ga_2(NMe_2)_6$, and water at 250 °C. A recent paper reported that ALD growth from $Gd(C_5H_4Me)_3$ and water afforded high purity Gd_2O_3 films at 250 °C.[22] However, the growth rate increased with $Gd(C_5H_4CH_3)_3$ pulse length and substrate temperature between 150 and 350 °C, and no ALD window was observed. Since the binary ALD process employing $Er(C_5H_4Me)_3$ and water affords surface limited growth at 250 °C[17] and because other lanthanide ions are likely to provide useful passivating layers for GaAs,[5,14] we chose to investigate the ALD growth of $Er_xGa_{2-x}O_3$ films from $Er(C_5H_4Me)_3$, $Ga_2(NMe_2)_6$, and water at 250 °C.

The use of TOF-ERDA has enabled us to quantify precisely the amount of light elements present (Table 1). The very low carbon, hydrogen, and nitrogen levels found for films from $Er(thd)_3$, $Ga(acac)_3$, and ozone probably result from a combination of the high reactivity of ozone, which eliminates these light elements as oxidized species that are efficiently swept from the growing film, and the high deposition temperature, which promotes efficient surface reactions. Trace levels of fluorine were observed in films grown from $Er(thd)_3$, $Ga(acac)_3$, and ozone. This is a common occurrence for high temperature ozone-based ALD processes using our reactor type, and is likely a result of ozone attacking the fluorocarbon lubricant used on the seals.[12] Fluorine contamination could be avoided by using hydrocarbon grease in place of the fluorocarbon lubricant. The carbon, hydrogen, and nitrogen levels for films deposited from $Er(C_5H_4Me)_3$, $Ga_2(NMe_2)_6$, and water decreased with increasing erbium content, which suggests that $Ga_2(NMe_2)_6$ may be contributing disproportionately to the incorporation of these elements. It has been documented that dialkylamido ligands can undergo thermally induced β-hydride elimination, which leads to intermediates containing imino ligands.[23] Such species possess direct metal–carbon bonds, and have been previously proposed as a source of carbon contamination in films grown from dialkylamido-based precursors.[23a] The use of water as a precursor may also be a major contributor of hydrogen impurities to the films.

In addition to the novelty of the thin film materials presented in this work, our processes represent a significant advancement toward the development of a viable passivator and dielectric for use in compound semiconductors. In a series of recent papers, it was reported that incorporation of gadolinium into Ga_2O_3 films resulted in greatly improved dielectric performance relative to pure Ga_2O_3 films, which were described as having poor electrical leakage and passivation properties.[4,5] It was also reported that $Gd_xGa_{2-x}O_3$ provided a very low interfacial state density (D_{it}) relative to dielectric materials such as SiO_2, Al_2O_3, and MgO, and that a low D_{it} is critical for MOSFETs in III–V semiconductor devices. The presence of gadolinium was proposed to play a crucial role as an electropositive stabilizing element, effectively fixing gallium in the 3+ oxidation state and preventing the formation of gallium suboxides, which were proposed to degrade performance.[5] It was also suggested that rare earth elements in general could act to stabilize Ga_2O_3.[5] Considering that lanthanide oxides are recognized high-κ dielectric materials and have similar chemical and physical characteristics,[14] it is probable that other $Ln_xGa_{2-x}O_3$ phases will function equally well as passivating dielectric materials.

Kwo and coworkers reported the leakage current density (J_L) of a series of MBE-grown $Gd_xGa_{2-x}O_3$ films with varying gadolinium content. For samples containing between 6 and 20% Gd, very low J_L values of 1–10 nA cm^{-2} were reported,[5d,e] which are comparable to those measured in our study (16 nA cm^{-2} for the $Er(thd)_3$, $Ga(acac)_3$, and ozone process, 17–26 nA cm^{-2} for the $Er(C_5H_4Me)_3$, $Ga_2(NMe_2)_6$, and water process). We also measured permittivity (κ) values of 10.8–11.3 for the $Er(thd)_3$, $Ga(acac)_3$, and ozone process and 9.2–10.4 for the $Er(C_5H_4Me)_3$, $Ga_2(NMe_2)_6$, and water process. These κ values are slightly lower than those reported for Er_2O_3 (κ = 13.0) and Gd_2O_3 (κ = 13.6),[24] and suggest that $Er_xGa_{2-x}O_3$ and other $Ln_xGa_{2-x}O_3$ are potential gate dielectric materials. Permittivity values were not reported in any of the $Gd_xGa_{2-x}O_3$ MBE papers. Our V_{fb} values appear to indicate a trend of increasing positive shift with smaller amounts of erbium present. This is consistent with the assertion made by Hong and coworkers that the lanthanide metal prevents the formation of gallium suboxides, which would provide a source of negative fixed charge.[5d–f] The $Er(thd)_3$, $Ga(acac)_3$, and ozone process afforded films with low amounts of carbon and hydrogen, compared to films obtained from the $Er(C_5H_4Me)_3$, $Ga_2(NMe_2)_6$, and water process. It is likely that the carbon and hydrogen contaminants in the latter are a source of charge traps leading to the larger ΔV_{fb} and reduced κ values, compared to the $Er(thd)_3$, $Ga(acac)_3$, and ozone process. The impurities may also provide the negative fixed charge responsible for the larger V_{fb} values.

Conclusions

The ALD growth of $Er_xGa_{2-x}O_3$ films was demonstrated using $Er(thd)_3$, $Ga(acac)_3$, and ozone and $Er(C_5H_4Me)_3$, $Ga_2(NMe_2)_6$, and water at substrate temperatures of 350 and 250 °C, respectively. Both processes provided uniform films and exhibited surface-limited ALD growth. The erbium : gallium ratios in the films could be adjusted by the pulse sequences of the erbium and gallium precursors. The $Er(thd)_3$, $Ga(acac)_3$, and ozone precursor system provided stoichiometric $Er_xGa_{2-x}O_3$ films with carbon, hydrogen, nitrogen, and fluorine levels of $<$0.2, $<$0.2, $<$0.3, and 0.6–2.2 atomic percent, respectively, with growth rates between 0.25 and 0.28 Å cycle^{-1}. The effective permittivities of representative samples from this precursor system were 10.8–11.3. The $Er(C_5H_4Me)_3$, $Ga_2(NMe_2)_6$ and water precursor system provided stoichiometric $Er_xGa_{2-x}O_3$ films with carbon,

hydrogen, nitrogen, and fluorine levels of 2.0–6.1, 5.0–10.3, <0.3–0.7, and ⩽0.1 atom percent, respectively, with growth rates between 1.0 and 1.5 Å cycle^{-1}. The growth rates varied as a function of the $Er(C_5H_4Me)_3$: $Ga_2(NMe_2)_6$ pulse ratio. The effective permittivities of representative samples from this precursor system were 9.2–10.4. The as-deposited films of both precursor systems were amorphous, but annealing between 900 and 1000 °C under a nitrogen atmosphere led to crystallization either to $Er_3Ga_5O_{12}$ or to a mixture of β-Ga_2O_3 and $Er_3Ga_5O_{12}$. Atomic force microscopy showed rms surface roughnesses of <1.0 nm for typical films regardless of precursor system or film composition.

Experimental

$Er_xGa_{2-x}O_3$ film deposition

An F-120 flow-type hot-walled ALD reactor manufactured by ASM Microchemistry Ltd was used for the thin film deposition experiments. The reactor was operated under a flow of nitrogen at a pressure of 2–3 mbar. The deposition of $Er_xGa_{2-x}O_3$ thin films by ALD was studied employing the two precursor systems described above. For each precursor system, metal source compound pulses were followed by an oxygen source pulse to afford the growth of an atomic layer of the corresponding metal oxide. By combining the individual metal oxide processes and adjusting the proportion of Er_2O_3 cycles relative to the number of Ga_2O_3 cycles, $Er_xGa_{2-x}O_3$ thin films were grown over a range of compositions, where $0 \leqslant x \leqslant 2$. $Ga_2(NMe_2)_6$ was obtained from the Aldrich Chemical Company and $Er(C_5H_4Me)_3$ was obtained from the Institute of Organometallic Chemistry, Russian Academy of Sciences, Nizhniy-Novgorod, Russia. Both were used as received. Due to the highly oxygen and moisture sensitive nature of $Ga_2(NMe_2)_6$ and $Er(C_5H_4Me)_3$, the compounds were stored and handled under argon in a glove box and exposure to air was avoided during transfer to the reactor through use of an air-free precursor transfer vessel. $Ga(acac)_3$ was obtained from Strem Chemicals Inc. and was used as received. $Er(thd)_3$ was prepared by a method described previously,[25] and was purified by sublimation under reduced pressure.

Precursor sublimation temperatures, pulse lengths, and purge lengths used in initial film growth experiments were selected from the parameters reported previously for the individual metal oxide processes[15–18] and were then optimized for use in the current study. $Ga_2(NMe_2)_6$, $Er(C_5H_4Me)_3$, $Ga(acac)_3$, and $Er(thd)_3$ were sublimed from open glass crucibles at 72, 112, 125, and 130 °C, respectively. Nitrogen (99.999+%) was used as both the carrier and purge gas and was obtained from air using a Nitrox UHPN 3000-1 nitrogen generator. Ozone was produced from 99.999+% O_2 using a Fischer Model 502 ozone generator. Water vapor was delivered from an external source container under its own vapor pressure at room temperature. Films were deposited onto 5 × 5 cm pieces cut from 150 mm Si(100) wafers obtained from Okmetic (Vantaa, Finland). Two substrates were used in each deposition experiment, with one positioned at the leading end and the other at the trailing end of the deposition zone, which effectively created a 5 × 10 cm substrate area. The native oxide was not removed prior to deposition.

Film characterization methods

Film thicknesses were determined by the fitting of reflectance spectra collected between 1100 and 190 nm, using a method described previously.[26] These reflectance spectra were measured using a Hitachi U-2000 double beam spectrophotometer. The thickness of the films was also determined in some cases from the fitting of X-ray reflectivity data collected on a parallel beam Bruker D8 Advance X-ray diffractometer. The film growth rate was determined by dividing the measured film thickness by the number of deposition cycles performed. X-Ray diffraction spectra were collected with a Philips MPD 1880 diffractometer using Cu Kα radiation. Atomic force micrographs were obtained using a Digital Instruments Nanoscope III atomic force microscope, and were performed in the tapping mode with a scan rate of 1.0 Hz. Surface roughnesses were calculated as rms values.

Composition analyses of representative $Er_xGa_{2-x}O_3$ thin films were performed using RBS and TOF-ERDA at the Accelerator Laboratory of IMEC (Leuven, Belgium). In TOF-ERDA experiments, heavy ions are accelerated and projected into the sample.[27] When high-energy ions hit the sample, elastic collisions result and recoils of the sample atoms are detected. Timing gates and charged particle detectors were used to determine recoil velocity and energy, respectively, which enabled mass separation. Analyses on the films described herein employed 48 MeV $^{79}Br^{9+}$ ions obtained from a 5 MV EGP-10-II tandem accelerator using a 38.5° angle of incidence. The elemental compositions reported were obtained directly from the total recoil yields using Rutherford scattering cross sections. RBS was performed with 1.0 MeV $^4He^{2+}$ ions at a 162° angle of incidence. Analysis of the RBS data gave precise erbium : gallium ratios and the ERDA data were used to afford precise metal-to-oxygen ratios and light element concentrations. For routine measurements, the erbium : gallium ratios were determined with a Philips W 1480 X-ray fluorescence spectrophotometer equipped with a rhodium X-ray tube. Data analyses were performed with the UNIQUANT 2.5 program, which employs a DJ Kappa model to calculate the composition and mass thickness of an unknown bulk or thin film sample.

Capacitance–voltage (*C–V*) and current–voltage (*I–V*) characteristics of the films were determined for samples deposited onto native oxide-covered p-type Si(100) substrates. Measurements were carried out for as-deposited films at room temperature and under normal pressure. Aluminium dots (0.204 mm^2) for ohmic contacts were electron beam evaporated onto the sample surface and reverse of the silicon substrates. The native silicon dioxide layer on the reverse was removed by HF-etching before the evaporation of aluminium. *C–V* and *I–V* measurements on the resulting Al/$Er_xGa_{2-x}O_3$/native SiO_2/p-silicon(100)/Al structures were carried out using an HP 4284A precision LCR-meter and Keithley 2400 source meter, respectively. In the *C–V* measurements, an AC signal frequency of 500 kHz, a voltage step size of 0.05 V, and delay time of 0.5 s between the steps were applied, and the Al top electrode was negatively biased in relation to the silicon substrate.

Acknowledgements

Efforts at Wayne State University were supported by the U.S. Army Research Office (grant no. W911NF-04-1-0332). The authors at the Helsinki University of Technology gratefully acknowledge the Academy of Finland for research funding (Projects 204742 and 205777). The authors would also like to thank Prof. P. Hautojärvi (HUT, Department of Physics) for the use of his AFM, Dr J. Niinistö (HUT, our lab) for performing AFM measurements, and Drs K. Kukli and J. Niinistö for assistance with electrical characterization.

References

1 For examples, see: D. S. Gill, R. W. Eason, J. Mendiola and P. J. Chandler, *Mater. Lett.*, 1995, **25**, 1.
2 For examples, see: (*a*) J. M. Phillips, *J. Appl. Phys.*, 1996, **79**, 1874; (*b*) E. A. Giess, R. L. Sandstrom, W. J. Gallager, A. Gupta, S. L. Shinde, R. F. Cook, E. I. Cooper, E. J. M. O'Sullivan, J. M. Roldan, A. P. Segmüller and J. Angilello, *IBM J. Res. Dev.*, 1990, **34**, 916.
3 For examples, see: (*a*) T. Ishihara, T. Yamada, H. Arikawa, H. Nishiguchi and Y. Takita, *Solid State Ionics*, 2000, **135**, 631; (*b*) D. Lybye, F. W. Poulsen and M. Mogensen, *Solid State Ionics*, 2000, **128**, 91; (*c*) T. Ishihara, J. A. Kilner, M. Honda and Y. Takita, *J. Am. Chem. Soc.*, 1997, **119**, 2747.
4 For examples, see: (*a*) M. Hong, K. A. Anselm, J. Kwo, H. M. Ng, J. N. Baillargeon, A. R. Kortan, J. P. Mannaerts, A. Y. Cho, C. M. Lee, J. I. Chyi and T. S. Lay, *J. Vac. Sci. Technol., B*, 2000, **18**, 1453; (*b*) S. Pal, S. K. Ray, S. Lahiri and D. N. Bose, *Electron. Lett.*, 2000, **36**, 2044; (*c*) F. Ren, J. M. Kwo, M. Hong, W. S. Hobson, J. R. Lothian, J. Lin, H. S. Tsai, J. P. Mannaerts, J. Kwo, S. N. G. Chu, Y. K. Chen and A. Y. Cho, *IEEE Electron Device Lett.*, 1998, **19**, 309; (*d*) F. Ren, M. Hong, S. N. G. Chu, M. A. Marcus, M. J. Schurman, A. Baca, S. J. Pearton and C. R. Abernathy, *Appl. Phys. Lett.*, 1998, **73**, 3893.
5 For examples and leading references, see: (*a*) M. Passlack, N. Medendorp, S. Zollner, R. Gregory and D. Braddock, *Appl. Phys. Lett.*, 2004, **84**, 2521; (*b*) V. V. Afanas'ev, A. Stesmans, M. Passlack and N. Medendorp, *Appl. Phys. Lett.*, 2004, **85**, 597; (*c*) M. Passlack, M. Medendorp, R. Gregory and D. Braddock, *Appl. Phys. Lett.*, 2003, **83**, 5262; (*d*) J. Kwo, D. W. Murphy, M. Hong, J. P. Mannaerts, R. L. Opila, R. L. Masaitis and A. M. Sergent, *Appl. Phys. Lett.*, 1999, **17**, 1294; (*e*) J. Kwo, D. W. Murphy, M. Hong, R. L. Opila, J. P. Mannaerts, A. M. Sergent and R. L. Masaitis, *Appl. Phys. Lett.*, 1999, **75**, 1116; (*f*) M. Hong, M. Passlack, J. P. Mannaerts, J. Kwo, S. N. G. Chu, N. Moriya, S. Y. Hou and V. J. Fratello, *J. Vac. Sci. Technol., B*, 1996, **14**, 2297.
6 For a review of GaAs semiconductor properties, see: J. S. Blakemore, *J. Appl. Phys.*, 1982, **53**, R123.
7 (*a*) A. M. Green and W. E. Spicer, *J. Vac. Sci. Technol., A*, 1993, **11**, 1061; (*b*) M. Hong, J. Kwo, A. R. Kortan, J. P. Manneaerts and A. M. Sergent, *Science*, 1999, **283**, 1897; (*c*) J. Kwo, M. Hong, B. Busch, D. A. Muller, Y. J. Chabal, A. R. Kortan, J. P. Mannaerts, B. Yang, P. Ye, J. Gossmann, A. M. Sergent, K. K. Ng, J. Bude, W. H. Schulte, E. Garfunkel and T. Gustafsson, *J. Cryst. Growth*, 2003, **251**, 645.
8 J. S. Morrell, Z. B. Xue, E. D. Specht and D. B. Beach, *Mater. Res. Soc. Symp. Proc.*, 1999, **547**, 309.
9 X. F. Meng, F. S. Pierce, K. M. Wong, R. S. Amos, C. H. Xu, B. S. Deaver, Jr. and S. J. Poon, *IEEE Trans. Magn.*, 1991, **27**, 1638.
10 B. Han, D. Neumayer, D. L. Schulz, T. J. Marks, H. Zhang and V. P. Dravid, *Appl. Phys. Lett.*, 1992, **61**, 3047.
11 B. Han, D. Neumayer, T. J. Marks, D. A. Rudman, H. Zhang and V. P. Dravid, *Appl. Phys. Lett.*, 1993, **63**, 3639.
12 M. Nieminen, S. Lehto and L. Niinistö, *J. Mater. Chem.*, 2001, **11**, 3148.
13 Selected ALD review articles: (*a*) L. Niinistö, J. Päiväsaari, J. Niinistö, M. Putkonen and M. Nieminen, *Phys. Status Solidi A*, 2004, **201**, 1443; (*b*) M. Leskelä and M. Ritala, *Angew. Chem., Int. Ed.*, 2003, **42**, 5548; (*c*) H. Kim, *J. Vac. Sci. Technol., B*, 2003, **21**, 2231; (*d*) M. Leskelä and M. Ritala, *Thin Solid Films*, 2002, **409**, 138; (*e*) L. Niinistö, *Curr. Opin. Solid State Mater. Sci.*, 1998, **3**, 147; (*f*) T. Suntola, *Thin Solid Films*, 1992, **216**, 84.
14 For leading references, see: (*a*) M. Leskelä, K. Kukli and M. Ritala, *J. Alloys Compd.*, 2006, **418**, 27; (*b*) J. Päiväsaari, M. Putkonen and L. Niinistö, *Thin Solid Films*, 2005, **472**, 275; (*c*) M. Leskelä and M. Ritala, *J. Solid State Chem.*, 2003, **171**, 170.
15 J. Päiväsaari, M. Putkonen, T. Sajavaara and L. Niinistö, *J. Alloys Compd.*, 2004, **374**, 124.
16 M. Nieminen, L. Niinistö and E. Rauhala, *J. Mater. Chem.*, 1996, **6**, 27.
17 J. Päiväsaari, J. Niinistö, K. Arstila, K. Kukli, M. Putkonen and L. Niinistö, *Chem. Vap. Deposition*, 2005, **11**, 415.
18 C. L. Dezelah, IV, J. Niinistö, K. Arstila, L. Niinistö and C. H. Winter, *Chem. Mater.*, 2006, **18**, 471.
19 Inorganic Phases, JCPDS-International Centre for Diffraction Data, Swarthmore, PA, 1988, Monoclinic β-Ga_2O_3 Card No. 11-370, Cubic $Er_3Ga_5O_{12}$ Card No. 12-769.
20 E. H. Nicollian and J. R. Brews, *MOS (Metal Oxide Semiconductor) Physics and Technology*, Wiley, New York, 1982, p. 466.
21 *International Technology Roadmap for Semiconductors*, 2005 edition, Semiconductor Industry Association, available electronically at: http://public.itrs.net/.
22 J. Niinistö, N. Petrova, M. Putkonen, L. Niinistö, K. Arstila and T. Sajavaara, *J. Cryst. Growth*, 2005, **285**, 191.
23 Leading references: (*a*) C. H. Winter, *Aldrichim. Acta*, 2000, **33**, 3; (*b*) D. C. Bradley and I. M. Thomas, *Can. J. Chem.*, 1962, **40**, 1355; (*c*) Y. Takahashi, N. Onoyama, Y. Ishikawa, S. Motojima and K. Sugiyama, *Chem. Lett.*, 1978, 525.
24 D. Xue, K. Betzler and H. Hesse, *J. Phys.: Condens. Matter*, 2000, **12**, 3113.
25 K. J. Eisentraut and R. E. Sievers, *J. Am. Chem. Soc.*, 1965, **87**, 5254.
26 M. Ylilammi and T. Ranta-aho, *Thin Solid Films*, 1993, **232**, 56.
27 M. Putkonen, T. Sajavaara, L. Niinistö and J. Keinonen, *Anal. Bioanal. Chem.*, 2005, **382**, 1791.